Near Real-Time Forest Loss Detection in the Brazilian Amazon Using Bayesian Fusion of Sentinel-1 SAR and Sentinel-2 Multispectral Time Series

Marta Bottani[1,2], Laurent Ferro-Famil[1,2]

[1] CESBIO, 18 avenue Edouard Belin, 31400, Toulouse, France - marta.bottani@utoulouse.fr
[2] ISAE Supaero, 10 Avenue Marc Pélegrin, 31400, Toulouse, France - laurent.ferro-famil@isae-supaero.fr

Keywords: Deforestation, Satellite Remote Sensing, Bayesian Method, Multi-Source Fusion, Sentinel-1, Sentinel-2.

Abstract

Timely and accurate detection of deforestation is essential for managing tropical forests, yet individual Earth observation sensors have inherent limitations. Multispectral imagery offers detailed spectral information on vegetation properties but is frequently hindered by cloud cover, while Synthetic Aperture Radar (SAR) imagery provides insights on vegetation structure independent of weather conditions but is sensitive to moisture variability and residual vegetation post-clearing. The complementary nature of these data has motivated multi-source fusion approaches, though most existing methods rely on offline processing or decision-level integration, limiting their real-time applicability. This study generalizes a Bayesian Online Changepoint Detection (BOCD) framework based on the recursive estimation of the number of acquisitions since the last change to asynchronous, irregularly sampled Sentinel-1 SAR and Sentinel-2 multispectral time series. A dynamically weighted fusion mechanism is implemented, in which each sensor's relevance reduces with increasing time since its last observation, according to a physical decay model. The resulting method, named ms-BOCD, enables interpretable, and Near Real-Time (NRT) detection of forest loss. The ms-BOCD method is validated using MapBiomas Alerta reference data spanning deforestation polygons ranging from 0.1 to 50 hectares in the Brazilian Amazon. Compared to VH-BOCD (BOCD using Sentinel-1 cross-polarization only) and the operational RADD and TropiSCO systems, ms-BOCD achieves a $\sim 25\%$ improvement in detection performance and maintains 13% fewer false alarms than Global Forest Watch (GFW), a platform that aggregates multiple independent deforestation alert products. Overall, these results demonstrate the strong potential of multi-source Bayesian fusion for operational tropical forest monitoring.

1. Introduction

Deforestation poses a critical threat to the Earth's climate system, making rapid monitoring crucial for implementing conservation measures and mitigating further environmental damages (Forzieri et al., 2022). In this context, satellite remote sensing offers a powerful means to monitor forest conditions at large scales and to track deforestation dynamics (Baker et al., 2010). Over the past years, numerous forest disturbance detection methods with Near Real-Time (NRT) capabilities have been developed, leveraging either multispectral (Verbesselt et al., 2010, Hansen et al., 2016) or Synthetic Aperture Radar (SAR) imagery (Bouvet et al., 2018, Reiche et al., 2018b, Doblas et al., 2020, Watanabe et al., 2018, Mullissa et al., 2023, Bottani et al., 2025a). Nowadays, several of these approaches have transitioned into operational systems deployed at different spatial scales. For example, the Global Land Analysis and Discovery (GLAD) system, originally based on Landsat imagery (GLAD-L) and later adapted to process Sentinel-2 data (GLAD-S2) (Hansen et al., 2016), is now fully operational across tropical and subtropical regions. Similarly, the JJ-FAST system, developed by JAXA and based on ALOS/PALSAR-2 SAR data, exploits multiple polarization channels to detect deforestation from distinct radar scattering characteristics (Watanabe et al., 2021), and is operational across several tropical countries. Several other operational systems rely on Sentinel-1 SAR data. Among them, the RADD system uses a Bayesian updating algorithm to compute deforestation probabilities and has been deployed in multiple tropical regions (Reiche et al., 2021). A similar probabilistic update strategy, combined with machine learning techniques, has also been employed to develop a global monitoring system named LUCA (Mullissa et al., 2024). In the Brazilian Amazon, the DETER-R system, developed by INPE, employs adaptive linear thresholding for forest loss detection (Doblas et al., 2022). Another example is TropiSCO, developed by CNES, which identifies forest loss events by detecting shadows that form along the boundaries between intact forests and recently cleared areas in several tropical countries (Mermoz et al., 2021, Ballère et al., 2021).

Despite these advances, existing methods remain constrained to single-sensor data—either SAR or multispectral—each with its own inherent limitations. Multispectral imagery is affected by cloud cover, and limited to surface observations due to low penetration capability. SAR data, in turn, are affected by speckle, geometric distortions in hilly regions, and sensitivity to variations in soil moisture and residual vegetation remaining after clearing. To address these limitations and enhance forest surveillance, data from multiple sensors can be combined to leverage their complementary physical principles (Erasmi and Twele, 2009, Reiche et al., 2013). Early offline multi-source fusion efforts primarily focused on land-use classification within probabilistic frameworks that explicitly accounted for asynchronous sensor acquisitions (Solberg et al., 1994, Bruzzone et al., 1999, Waske and Benediktsson, 2007). More recently, several approaches have been developed to enable multi-sensor forest loss monitoring. One pixel-based method fuses Landsat Normalized Difference Vegetation Index (NDVI) with ALOS PALSAR backscatter time series to detect historical deforestation, improving both spatial and temporal accuracy compared to using either dataset alone (Reiche et al., 2015). A Bayesian multitemporal framework has also been extended to integrate Landsat and ALOS PALSAR mosaics by converting both data types into forest probability estimates (Lehmann et al., 2015), allowing the analysis of a unified signal rather than treating

This contribution has been peer-reviewed. The double-blind peer-review was conducted on the basis of the full paper.
https://doi.org/10.5194/isprs-annals-XI-3-2026-507-2026

multispectral and SAR observations separately. Furthermore, an algorithm integrating Sentinel-1 with ALOS-2 PALSAR-2 and Landsat-7/8 data has been proposed to compute NRT deforestation probabilities (Reiche et al., 2018a). Another approach exploits dense time series and machine learning models to combine sensor-specific disturbance probabilities at the pixel level (Shimizu et al., 2019), while a complementary strategy generates separate disturbance maps for each sensor and merges them through a union process (Hirschmugl et al., 2020). Despite the extensive literature, most existing methods rely on offline processing or decision-level fusion strategies, which do not fully exploit the temporal and spectral synergies between the two data sources. Consequently, no operational forest loss monitoring system currently integrates both modalities within a truly unified framework. Global Forest Watch (GFW) is the only existing operational platform that aggregates deforestation alerts from multiple monitoring systems (Reiche et al., 2024); however, this *a posteriori* aggregation also tends to accumulate false detections (Bottani et al., 2025a).

In this context, the present work introduces a generalized Bayesian online changepoint detection framework, named ms-BOCD, designed to process asynchronous and unequally sampled time series from multiple sensors. The method integrates Sentinel-1 SAR backscatter and Sentinel-2 NDVI observations within a single Markov chain that models the number of acquisitions since the last detected change, referred to as the run length (Adams and MacKay, 2007). Contributions from each data source are weighted to gradually reduce the influence of outdated observations, allowing the method to dynamically adapt to new information. Change detection is performed recursively using an online Maximum *a Posteriori* (MAP) estimation of the run length, indicating deforestation events. The ms-BOCD method is tested for forest loss detection in the Brazilian Amazon using reference data of deforested areas with sizes ranging from 0.1 to 50 hectares. The results are further compared to those from several existing methods, including SAR-based BOCD, RADD, TropiSCO, and GFW.

The remainder of this paper is organized as follows. Section 2 introduces the study area and describes the input and reference data used for validation. Section 3 provides an overview of Bayesian online changepoint detection and introduces a generalization of the framework for multi-source fusion. Section 4 presents and discusses the spatial and temporal performance of ms-BOCD in comparison with deforestation alerts from existing operational systems. Finally, Section 5 provides concluding remarks and outlines future perspectives.

2. Study Area and Data

The study area for this work is the Brazilian Amazon, which covers approximately 5 million square kilometers in northern Brazil. The region is dominated by evergreen tropical forests and hosts exceptionally high biodiversity. Between 2019 and 2022, 6.5 million hectares were deforested in the Amazon, primarily due to large-scale agricultural expansion (RAD2023, 2024). While large clearings account for most of the total deforestation, small-scale disturbances are becoming increasingly prevalent, often linked to artisanal mining, illegal logging, and subsistence agriculture (Kalamandeen et al., 2018). These finer-scale clearings contribute significantly to biodiversity loss and often serve as precursors to more extensive deforestation.

Table 1. Characteristics of the input data.

Feature	Sentinel-1 (S1)	Sentinel-2 (S2)
Satellite	S1A/S1B	S2A/S2B
Image product	RTC	L2A
Relevant bands / polarization	VH	B4 (red), B8 (NIR)
Spatial resolution	$\approx 20 \times 22$ m	10 m
Revisit time	6 days	5 days

2.1 Input Data

The input data used in this work consist of Sentinel-1 (S1) A/B C-band Radiometrically Terrain Corrected (RTC) imagery, acquired in Interferometric Wide Swath (IW) mode and in cross-polarization (VH). No speckle filtering is applied to the Sentinel-1 data, resulting in an equivalent number of looks (ENL) of approximately 4.4. Additionally, Sentinel-2 (S2) Level-2A products are used to compute NDVI (Tucker, 1979). The main characteristics of the input data sources are summarized in Table 1.

2.2 Reference Data

The reference data used in this study are provided by MapBiomas Alerta (MBA) (RAD2023, 2024), which is an organization that validates deforestation alerts from multiple operational forest loss monitoring systems in Brazil through visual inspection of high-resolution optical imagery. The MBA dataset includes deforested polygons with key attributes such as clearing size, type of land conversion, and pre- and post-deforestation dates. The detection principle used in this study is based on the overlap between polygons. In particular, a disturbed region is considered detected when a significant portion of its area, i.e., T_{poly}, is identified as forest loss by the proposed method:

$$\frac{A_{\text{detected}}}{A_{\text{polygon}}} \geq T_{\text{poly}}, \tag{1}$$

where A_{detected}: area detected by the proposed method;
A_{polygon}: area of the reference MBA polygon;
T_{poly}: threshold.

Validation is performed for the monitoring year 2020. To mitigate potential bias arising from disturbed areas not detected in the MBA dataset, true positives are calculated using the 2020 reference data, whereas false positives are estimated through a temporal approach. Specifically, any area flagged as deforested by MBA in a given year is excluded from analysis in subsequent years; accordingly, MBA polygons from 2021 are used to identify false positives for the 2020 evaluation. The reference dataset used in this study is derived from MBA through stratified sampling (Robb and Cochran, 1963) based on four predefined size categories: 0.1–1 ha, 1–5 ha, 5–20 ha, and 20–50 ha. Table 2 summarizes the number of reference polygons per size class employed to assess true and false positives, and the spatial distribution of the 2020 reference polygons is also illustrated in Figure 1.

3. Method

3.1 Overview of Bayesian Online Change Detection

Let $\mathbf{x}_{1:n} = (x_1, \cdots, x_n)$ be a data vector acquired from a single sensor and exhibiting a changepoint, as illustrated in

Table 2. Number of reference polygons by clearing size class. A: polygon area.

2020 Reference Dataset (True Positive)			
$0.1 \leq A_0 < 1$ ha	$1 \leq A_1 < 5$ ha	$5 \leq A_2 < 20$ ha	$20 \leq A_3 \leq 50$ ha
75	488	320	117
2021 Reference Dataset (False Positive)			
48	419	358	175

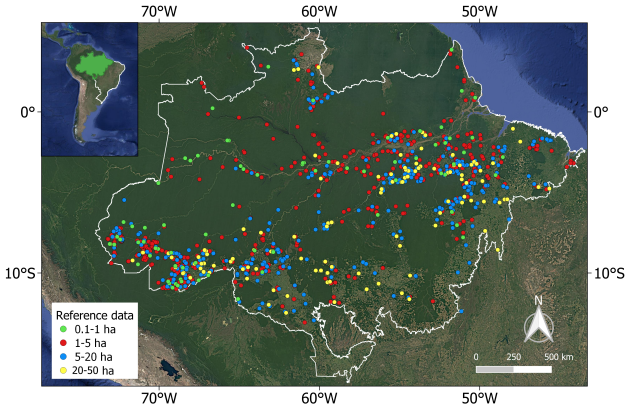

Figure 1. Spatial distribution of 2020 reference polygons extracted from MBA. Optical background ©2025 Google Earth.

Figure 2a. Bayesian Online Changepoint Detection (BOCD) is based on modeling the number of acquisitions since the last changepoint, referred to as the run length (Adams and MacKay, 2007). In particular, the run length at acquisition n, denoted by r_n (Figure 2b), increases linearly in the absence of a change and resets to 0 when a changepoint occurs. The objective of the algorithm is to estimate the *a posteriori* distribution of the run length, which can be expressed as follows:

$$p(r_n|\mathbf{x}_{1:n}) = \frac{p(r_n, \mathbf{x}_{1:n})}{\sum_{r_n=0}^{t} p(r_n, \mathbf{x}_{1:n})}. \tag{2}$$

By treating the run length as the hidden state of a Markov model, the joint distribution can be expressed recursively as:

$$p(r_n, \mathbf{x}_{1:n}) = \sum_{r_{n-1}=0}^{n-1} \underbrace{p\left(x_n|\mathbf{x}_{n-1}^{(r_{n-1})}\right)}_{\text{Posterior predictive}} \underbrace{p(r_n|r_{n-1})}_{\text{Transition probability}} \underbrace{p(r_{n-1}, \mathbf{x}_{1:n-1})}_{\text{Message}}. \tag{3}$$

In (3), the message represents the recursive element of the algorithm, the transition probability is defined *a priori* and can be assumed constant for simplicity, while the posterior predictive distribution depends on the data likelihood. In particular, if the likelihood belongs to an exponential family of distributions, prior conjugacy can be employed, and the posterior predictive distribution can be determined through a simple parameter update (Fink, 1997).

At step n, the most probable run length, M_n, is given by:

$$M_n = \arg\max_{r_n} p(r_n|\mathbf{x}_{1:n}). \tag{4}$$

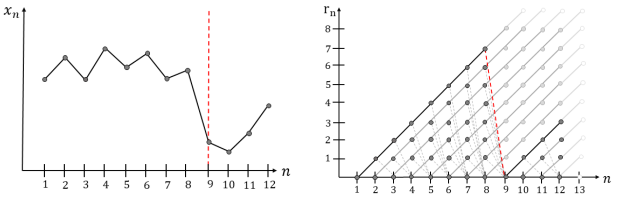

(a) Single sensor time series. (b) r_n map.

Figure 2. Illustrative example of run-length computation; changepoint marked with dashed red line.

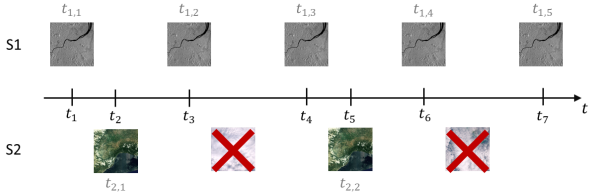

Figure 3. Illustration of a multi-source time series with asynchronous, unevenly spaced acquisitions. Cloudy multispectral images are excluded.

A change is detected when M_n drops, i.e., $M_n < M_{n-1} - \Delta M$, reaching a value that reflects the detection delay. The threshold $\Delta M > 0$ defines the minimum shift in M_n that can be interpreted as a meaningful change, ensuring robustness to minor oscillations arising from natural variability in the input data. Its value is determined empirically.

3.2 Multi-Source Fusion

This work generalizes the framework presented in Section 3.1 to multi-source fusion, hereafter referred to as ms-BOCD. Considering two sensors acquiring data at different times, the resulting time series is constructed by merging and sorting the acquisition dates of both sensors, as illustrated in Figure 3. The objective is to integrate this asynchronous and irregularly sampled time series into a single Markov chain that estimates (2) by recursively computing the components of (3) over time. In this context, particular attention must be given to the definition of the posterior predictive distribution in (3), which must be adapted to handle composite, multi-source observations.

Assuming that the sensors are independent between changepoints and are characterized by individual posterior predictive distributions, i.e., $p\left(x_{i,n_i} \mid \mathbf{x}_{i,n_i-1}^{(r_{n-1})}\right)$, $i = 1, 2$, where i denotes the sensor index, multi-source fusion requires defining a global posterior predictive distribution as a function of the individual ones:

$$p\left(\mathbf{x}_n \mid \mathbf{X}_{n-1}^{(r_{n-1})}\right) = \mathcal{G}\left\{p\left(x_{i,n_i} \mid \mathbf{x}_{i,n_i-1}^{(r_{n-1})}\right)\right\}_{i=1,2}. \tag{5}$$

In the ideal case of synchronous observations, multi-source fusion reduces to the standard multivariate formulation of Bayesian online changepoint detection, in which independent posterior predictive distributions are combined through their product between changepoints (Bottani and Ferro-Famil, 2025). However, when observations are asynchronous and irregularly sampled, the relevance of each data source to the current fusion time depends on its temporal proximity. As the temporal

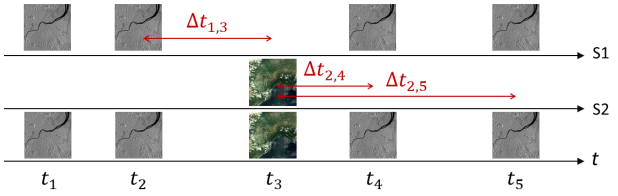

Figure 4. Example of computation of $\Delta t_{i,n}$ for two sensors.

gap since a sensor's last observation increases, its information content becomes progressively less representative of the current system state. If not accounted for, this can lead to false or delayed detections, particularly when one sensor is missing for an extended period.

One extreme fusion strategy consists of taking the product of the individual posterior predictive distributions at each time step. This corresponds to a full-memory approach, in which the posterior predictive of the most recently observed sensor is updated, while the posterior predictive of the other sensor is retained from its last observation. Conversely, a no-memory strategy considers only the latest observed sensor, thereby discarding potentially useful information from the other data source. While simple, both approaches are sub-optimal in the presence of asynchronous sampling.

To address this limitation, an intermediate fusion strategy motivated by physical considerations is adopted. In this formulation, multi-source fusion is performed through a weighted product of the individual posterior predictive distributions, allowing older observations to be progressively down-weighted:

$$p_{\mathbf{w}(r_{n-1})}\left(\mathbf{x}_n|\mathbf{X}_{n-1}^{(r_{n-1})}\right) = \prod_{i=1}^{2} p^{w_i(r_{n-1})}\left(x_{i,n_i} \mid \mathbf{x}_{i,n_i-1}^{(r_{n-1})}\right). \tag{6}$$

The weights w_i are defined deterministically as:

$$w_i(r_{n-1}) = e^{-\lambda \Delta t_{i,n}} \, \forall r_{n-1}, \quad \Delta t_{i,n} = t_n - t_{i,n_i} \geq 0, \tag{7}$$

where λ denotes a forgetting factor controlling the temporal decay of sensor relevance, and $\Delta t_{i,n}$ represents the time elapsed since the most recent observation of sensor i. An example illustrating the computation of $\Delta t_{i,n}$ is provided in Figure 4.

3.3 Algorithm Configuration

In this work, both Sentinel-1 backscatter and Sentinel-2 NDVI are assumed to be Gaussian distributed (Bottani et al., 2025a, León-López et al., 2022), which allows their individual posterior predictive distributions to be derived in closed form using prior conjugacy. This makes the algorithm extremely lightweight, as at each iteration only a set of parameters needs to be updated. Furthermore, to assess detection performance, ms-BOCD is implemented with an empirical $\Delta M = 10$, and $\lambda = 0.2$ is adopted following the sensitivity experiments reported in (Bottani et al., 2025b), which demonstrated stable detection performance across a range of decay rates.

4. Results

This section presents the spatial and temporal performance of ms-BOCD for forest loss detection, compared against existing approaches, using the reference data described in Section 2.2.

4.1 Spatial Performance

The detection results reported in Table 3 show that ms-BOCD achieves an overall 26% increase in detection performance compared to VH-BOCD (BOCD using Sentinel-1 cross-polarization only) at $T_{poly} = 75\%$, with especially strong improvements as the clearing size increases, i.e., +7% for A_0 to +27% for A_3. RADD and VH-BOCD achieve comparable results, with VH-BOCD outperforming RADD on small clearings, i.e., +33% for A_0, and RADD outperforming VH-BOCD on large clearings, i.e., +14% for A_3. TropiSCO achieves a modest 3% improvement over RADD and VH-BOCD at $T_{poly} = 75\%$, following similar trends to RADD across clearing size classes. GFW is largely affected by false detections, i.e., from +13% at $T_{poly} = 75\%$ to +25% at $T_{poly} = 10\%$, likely due to the *a posteriori* aggregation of deforestation alerts from multiple systems. The joint use of SAR and multispectral imagery in ms-BOCD leads to a modest increase in false alarms compared to VH-BOCD, i.e., +0.6% at $T_{poly} = 75\%$.

In general, the benefit of fusing multispectral and SAR information is particularly evident in detecting large clearings, which are typically associated with ”slash-and-burn” deforestation in the Amazon (Bezerra et al., 2024), where residual vegetation can remain on the ground for several months after clearing. In such cases, SAR data alone may struggle due to strong volume scattering that can saturate the signal, as illustrated in Figure 5, which shows examples of deforestation detections comparing ms-BOCD and VH-BOCD.

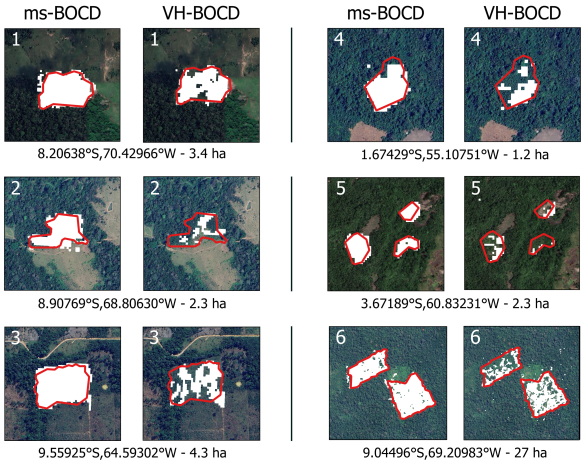

Figure 5. Examples of ms-BOCD and VH-BOCD detections of MBA reference polygons shown in red. Optical background ©2025 Google Earth.

4.2 Temporal Performance

The overall comparison of detection dates across all methods is shown as density curves in Figure 6, while Figure 7 presents the same comparison for ms-BOCD and VH-BOCD only, which performed the best, broken down by clearing size. Overall, ms-BOCD and VH-BOCD exhibit comparable performance,

Table 3. Detection performance of ms-BOCD compared to existing methods. A_0–A_3 defined in Table 2. T_{poly} defined in (1). “ALL” indicates performance over the entire dataset.

True Positive (TP) [%]																									
T_{poly}	ms-BOCD					VH-BOCD					RADD					TropiSCO					GFW				
	ALL	A_0	A_1	A_2	A_3	ALL	A_0	A_1	A_2	A_3	ALL	A_0	A_1	A_2	A_3	ALL	A_0	A_1	A_2	A_3	ALL	A_0	A_1	A_2	A_3
75%	58.9	78.7	66.4	46.4	46.6	33.1	72.0	37.0	23.6	19.8	33.6	38.7	36.5	27.8	34.2	36.5	44.0	40.4	30.0	33.3	69.2	80.0	70.3	65.0	69.2
50%	77.3	89.3	84.4	67.5	65.0	65.0	82.7	71.9	56.6	48.3	63.5	72.0	68.6	56.9	54.7	61.1	68.0	67.4	52.5	53.8	86.0	85.3	87.3	85.6	82.1
30%	87.3	93.3	91.5	81.8	79.6	78.9	90.7	84.2	70.8	71.6	77.1	80.0	80.1	75.3	67.5	76.2	77.3	80.5	72.2	68.4	91.5	89.3	92.0	92.5	88.0
10%	95.6	97.3	96.8	93.4	95.1	92.5	94.7	92.4	92.8	90.5	89.2	82.7	91.4	90.6	80.3	87.7	82.7	89.3	88.8	81.2	95.7	93.3	95.3	97.8	93.2
False Positive (FP) [%]																									
75%	0.6	1.5	0.2	1.4	0.0	0.0	0.0	0.0	0.0	0.0	0.0	0.0	0.0	0.0	0.0	0.0	0.0	0.0	0.0	0.0	13.8	10.6	12.4	14.2	17.1
50%	1.4	1.5	0.6	3.1	0.0	0.0	0.0	0.0	0.0	0.0	0.0	0.0	0.0	0.0	0.0	0.0	0.0	0.0	0.0	0.0	19.7	10.6	16.2	24.3	21.1
30%	3.4	7.4	2.4	4.4	2.1	0.0	0.0	0.0	0.0	0.0	0.3	0.0	0.5	0.3	0.0	0.2	0.0	0.2	0.3	0.0	27.9	17.0	22.4	34.1	31.4
10%	13.6	14.7	10.1	15.9	22.9	1.6	4.2	1.9	1.4	0.6	3.2	2.1	5.0	2.5	0.6	1.3	2.7	1.2	1.3	0.9	38.1	21.3	31.0	47.5	40.6

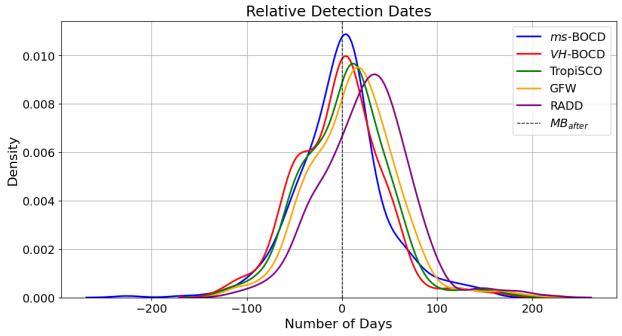

Figure 6. Density curves of detection dates for all considered methods relative to MBA ($t_{MB_{after}}$).

followed by TropiSCO, GFW, and RADD. The size-based analysis further shows that both VH-BOCD and ms-BOCD detect small-scale clearings (i.e., A_0 in Figure 7a) faster than MBA. As clearing size increases, detection speed relative to MBA generally decreases; however, ms-BOCD consistently maintains an advantage over VH-BOCD. This pattern likely reflects the slower and more gradual clearing processes associated with larger deforested areas.

4.3 Preliminary Results in Sparse Vegetation: Cerrado

To evaluate the potential generalizability of ms-BOCD beyond tropical rainforest ecosystems, the method is applied to a sparse vegetation environment in the Brazilian Cerrado. Figure 8 shows representative single-pixel time series for Sentinel-1 cross-polarization backscatter (i.e., γ^0_{VH}) and Sentinel-2 NDVI data, along with the corresponding posterior run-length probability matrices resulting from ms-BOCD detection. While not exhaustive, this analysis illustrates the potential of the framework to detect changes in heterogeneous, semi-open savannah formations, with successful detections and reasonable detection delays even in the presence of pronounced seasonality affecting both sources—particularly multispectral imagery—and periods of missing optical observations due to persistent cloud cover.

5. Conclusion

This study presents a multi-source generalization of a Bayesian online changepoint detection framework for forest loss monitoring, tested in the Brazilian Amazon. By integrating asynchronous and unequally sampled SAR and multispectral time series from Sentinel-1 and Sentinel-2, ms-BOCD effectively leverages complementary information from both sensors. The method was validated using reference data provided by MapBiomas Alerta, showing consistent improvements over single-source approaches, particularly for larger clearings where SAR-only detection is challenged by volume scattering associated with gradual deforestation practices that leave behind vegetation debris. Comparisons with existing methods, including RADD, VH-BOCD, TropiSCO, and GFW, demonstrated that ms-BOCD achieves higher detection rates while maintaining low false positive levels. A further analysis of temporal performance highlighted that ms-BOCD performs comparably to the SAR-only VH-BOCD in detecting smaller parcels, while showing an advantage for larger deforested areas.

Overall, these results highlight the potential of ms-BOCD for operational monitoring of tropical deforestation, providing a robust framework for integrating multi-sensor information while accommodating differences in temporal sampling. However, certain scenarios may limit its effectiveness: persistent cloud cover can reduce the contribution of optical data, atypical SAR responses (e.g., flooding or logging residues) may lead to misleading updates, and long temporal gaps between sensors can affect fusion accuracy. Additionally, very gradual clearings may be detected with some delay. To address these limitations, future work could explore the inclusion of additional SAR frequencies, such as L-band acquisitions (e.g., NISAR) and P-band data from the BIOMASS mission, which provide greater canopy penetration than C-band, as well as additional optical indices beyond NDVI. Incorporating these complementary sources would allow testing the flexibility of the multi-source fusion framework and may improve detection of forest disturbance dynamics across heterogeneous regions.

References

Adams, R. P., MacKay, D. J., 2007. Bayesian online changepoint detection.

Baker, D. J., Richards, G., Grainger, A., Gonzalez, P., Brown, S., DeFries, R., Held, A., Kellndorfer, J., Ndunda, P., Ojima, D., Skrovseth, P.-E., Souza, C., Stolle, F., 2010. Achieving forest carbon information with higher certainty: A five-part plan. *Environmental Science & Policy*, 13(3), 249-260.

Ballère, M., Bouvet, A., Mermoz, S., Toan, T. L., Koleck, T., Bedeau, C., André, M., Forestier, E., Frison, P.-L., Lardeux, C., 2021. SAR data for tropical forest disturbance alerts in French Guiana: Benefit over optical imagery. *Remote Sensing of the Environment*, 252, 112159.

Bezerra, J. S., Arroyo-Rodríguez, V., Arasa-Gisbert, R., Meave, J. A., 2024. Multiscale Effects of Slash-and-Burn Agriculture Across the Tropics: Implications for the Sustainability of an Ancestral Agroecosystem. *Sustainability*, 16(22).

Bottani, M., Ferro-Famil, L., 2025. Approche bayésienne pour la détection de la déforestation à partir de séries temporelles

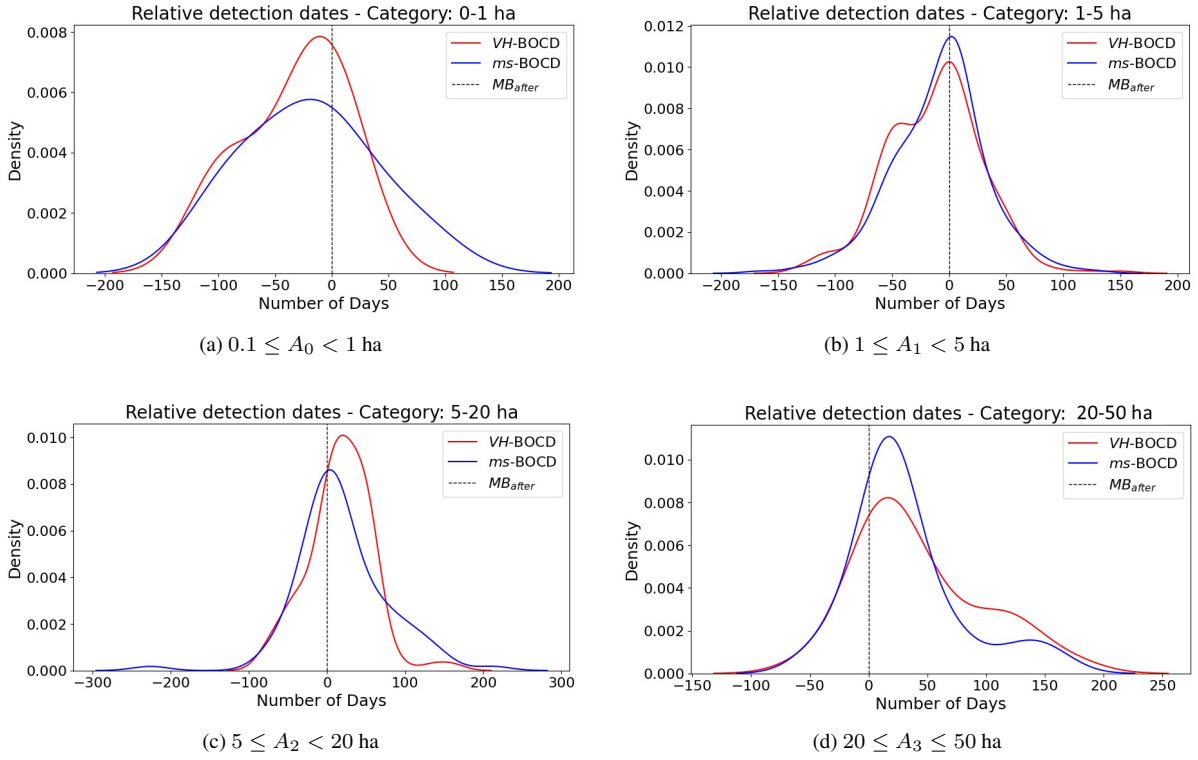

(a) $0.1 \leq A_0 < 1$ ha

(b) $1 \leq A_1 < 5$ ha

(c) $5 \leq A_2 < 20$ ha

(d) $20 \leq A_3 \leq 50$ ha

Figure 7. Density curves of detection dates for ms- and VH-BOCD methods relative to MBA ($t_{MB_{after}}$), per polygon size category.

d’images sar polarimétriques sentinel-1. *Proc. 30° Colloque sur le traitement du signal et des images*, Strasbourg, France, p. 917–920.

Bottani, M., Ferro-Famil, L., Doblas Prieto, J., Mermoz, S., Bouvet, A., Koleck, T., Le Toan, T., 2025a. Novel Unsupervised Bayesian Method for Near Real-Time Forest Loss Detection Using Sentinel-1 SAR Time Series: Assessment over Sampled Deforestation Events in Amazonia and the Cerrado. *Remote Sensing of Environment*, 331, 115037.

Bottani, M., Ferro-Famil, L., Tourneret, J.-Y., 2025b. Multisource fusion using bayesian online change detection: Application to deforestation monitoring using sar-optical time series. *Proc. IEEE International Workshop on Computational Advances in Multi-Sensor Adaptive Processing*, Punta Cana, Dominican Republic.

Bouvet, A., Mermoz, S., Ballère, M., Koleck, T., Toan, T. L., 2018. Use of the SAR Shadowing Effect for Deforestation Detection with Sentinel-1 Time Series. *Remote Sensing*, 10(8).

Bruzzone, L., Prieto, D., Serpico, S., 1999. A neural-statistical approach to multitemporal and multisource remote-sensing image classification. *IEEE Transactions on Geoscience and Remote Sensing*, 37(3), 1350-1359.

Doblas, J., Reis, M. S., Belluzzo, A. P., Quadros, C. B., Moraes, D. R. V., Almeida, C. A., Maurano, L. E. P., Carvalho, A. F. A., Sant’Anna, S. J. S., Shimabukuro, Y. E., 2022. DETER-R: An Operational Near-Real Time Tropical Forest Disturbance Warning System Based on Sentinel-1 Time Series Analysis. *Remote Sensing*, 14(15).

Doblas, J., Shimabukuro, Y., Sant’Anna, S., Carneiro, A., Aragão, L., Almeida, C., 2020. Optimizing near real-time detection of deforestation on tropical rainforests using Sentinel-1 data. *Remote Sensing*, 12(23).

Erasmi, S., Twele, A., 2009. Regional land cover mapping in the humid tropics using combined optical and SAR satellite data - A case study from Central Sulawesi, Indonesia. *International Journal of Remote Sensing*, 30, 2465-2478.

Fink, D., 1997. A compendium of conjugate priors. Technical report, Montana State Univeristy.

Forzieri, G., Dakos, V., McDowell, N. G., Ramdane, A., Cescatti, A., 2022. Emerging signals of declining forest resilience under climate change. *Nature*, 608, 534–539.

Hansen, M. C., Krylov, A., Tyukavina, A., Potapov, P. V., Turubanova, S., Zutta, B., Ifo, S., Margono, B., Stolle, F., Moore, R., 2016. Humid tropical forest disturbance alerts using Landsat data. *Environmental Research Letters*, 11(3), 034008.

Hirschmugl, M., Deutscher, J., Sobe, C., Bouvet, A., Mermoz, S., Schardt, M., 2020. Use of SAR and optical time series for tropical forest disturbance mapping. *Remote Sensing*, 12.

Kalamandeen, M., Gloor, M., Mitchard, E., Quincey, D., Ziv, G., Spracklen, D., Spracklen, B., Adami, M., Aragão, L., Galbraith, D., 2018. Pervasive Rise of Small-scale Deforestation in Amazonia. *Scientific Reports*, 8.

Lehmann, E. A., Caccetta, P., Lowell, K., Mitchell, A. L., Zhou, Z.-S., Held, A., Milne, T., Tapley, I., 2015. SAR and optical remote sensing: Assessment of complementarity and interoperability in the context of a large-scale operational forest monitoring system. *Remote Sensing of the Environment*, 156, 335-348.

León-López, K. M., Mouret, F., Arguello, H., Tourneret, J.-Y., 2022. Anomaly Detection and Classification in Multispectral Time Series Based on Hidden Markov Models. *IEEE Transactions on Geoscience and Remote Sensing*, 60, 1-11.

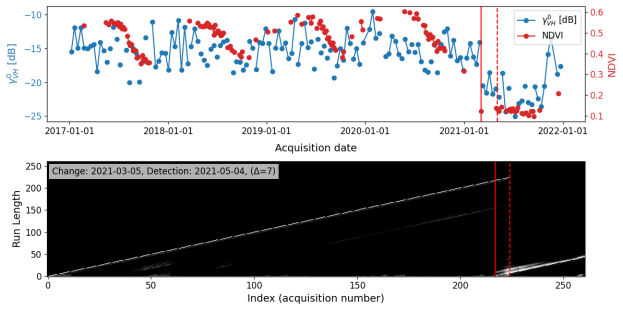

(a) Pixel location: (45.87606°W, 10.79773°S)

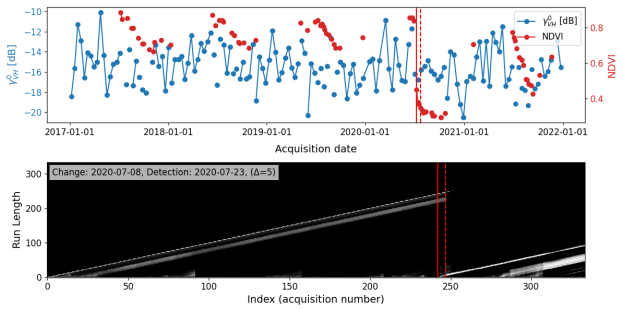

(b) Pixel location: (44.21158°W, 5.23681°S)

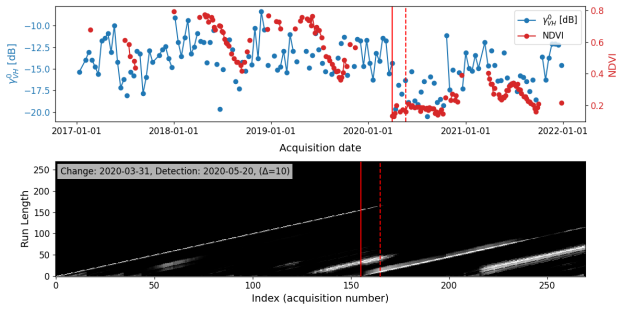

(c) Pixel location: (52.08677°W, 16.42960°S)

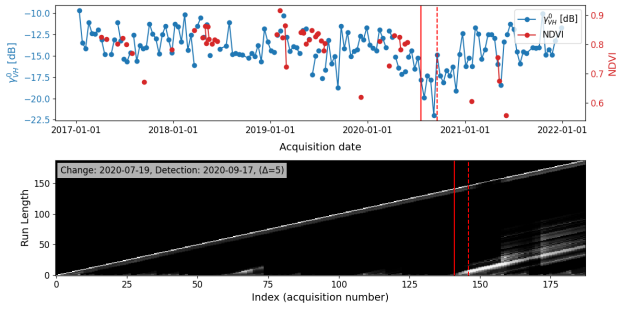

(d) Pixel location: (47.63699°W, 18.22273°S)

Figure 8. Examples of single-pixel backscatter and NDVI time series showing deforestation events (top) and posterior run length probabilities (bottom). Change dates are shown in solid red, detection dates in dashed red, and Δ indicates the detection delay in acquisitions.

Mermoz, S., Bouvet, A., Koleck, T., Ballère, M., Toan, T. L., 2021. Continuous Detection of Forest Loss in Vietnam, Laos, and Cambodia Using Sentinel-1 Data. *Remote Sensing*, 13(23).

Mullissa, A. G., Reiche, J., Herold, M., 2023. Deep learning and automatic reference label harvesting for Sentinel-1 SAR-based rapid tropical dry forest disturbance mapping. *Remote Sensing of the Environment*, 298, 113799.

Mullissa, A., Saatchi, S., Silva, R., Erickson, T., Provost, N., Osborn, F., Ashary, A., Moon, V., Melling, D., 2024. LUCA: A Sentinel-1 SAR-Based Global Forest Land Use Change Alert. *Remote Sensing*, 16, 2151.

RAD2023, 2024. Radd2023 :annual deforestation report of brazil 2023. Technical report, São Paulo, Brazil.

Reiche, J., Balling, J., Pickens, A. H., Masolele, R. N., Berger, A., Weisse, M. J., Mannarino, D., Gou, Y., Slagter, B., Donchyts, G., Carter, S., 2024. Integrating satellite-based forest disturbance alerts improves detection timeliness and confidence. *Environmental Research Letters*, 19.

Reiche, J., Hamunyela, E., Verbesselt, J., Hoekman, D., Herold, M., 2018a. Improving near-real time deforestation monitoring in tropical dry forests by combining dense Sentinel-1 time series with Landsat and ALOS-2 PALSAR-2. *Remote Sensing of the Environment*, 204(5), 147-161.

Reiche, J., Mullissa, A., Slagter, B., Gou, Y., Tsendbazar, N.-E., Odongo-Braun, C., Vollrath, A., Weisse, M. J., Stolle, F., Pickens, A., Donchyts, G., Clinton, N., Gorelick, N., Herold, M., 2021. Forest disturbance alerts for the Congo Basin using Sentinel-1. *Environmental Research Letters*, 16(2), 024005.

Reiche, J., Souza, C. M., Hoekman, D. H., Verbesselt, J., Persaud, H., Herold, M., 2013. Feature Level Fusion of Multi-Temporal ALOS PALSAR and Landsat Data for Mapping and Monitoring of Tropical Deforestation and Forest Degradation. *IEEE Journal of Selected Topics in Applied Earth Observations and Remote Sensing*, 6, 2159-2173.

Reiche, J., Verbesselt, J., Hoekman, D., Herold, M., 2015. Fusing Landsat and SAR time series to detect deforestation in the tropics. *Remote Sensing of the Environment*, 276-293.

Reiche, J., Verhoeven, R., Verbesselt, J., Hamunyela, E., Wielaard, N., Herold, M., 2018b. Characterizing tropical forest cover loss using dense Sentinel-1 data and active fire alerts. *Remote Sensing*, 10(5).

Robb, R., Cochran, G., 1963. Sampling Techniques (John Wiley & Sons, 2nd edition). *Proceedings of the Edinburgh Mathematical Society*, 102532.

Shimizu, K., Ota, T., Mizoue, N., 2019. Detecting Forest Changes Using Dense Landsat 8 and Sentinel-1 Time Series Data in Tropical Seasonal Forests. *Remote Sensing*, 11, 1899.

Solberg, A., Jain, A., Taxt, T., 1994. Multisource classification of remotely sensed data: fusion of Landsat TM and SAR images. *IEEE Transactions on Geoscience and Remote Sensing*, 32(4), 768-778.

Tucker, C. J., 1979. Red and photographic infrared linear combinations for monitoring vegetation. *Remote Sensing of the Environment*, 8, 127-150.

Verbesselt, J., Hyndman, R. J., Newnham, G. J., Culvenor, D., 2010. Detecting trend and seasonal changes in satellite image time series. *Remote Sensing of the Environment*, 114, 106-115.

Waske, B., Benediktsson, J. A., 2007. Fusion of Support Vector Machines for Classification of Multisensor Data. *IEEE Transactions on Geoscience and Remote Sensing*, 45(12), 3858-3866.

Watanabe, M., Koyama, C. N., Hayashi, M., Nagatani, I., Shimada, M., 2018. Early-stage deforestation detection in the tropics with L-band SAR. *IEEE Journal of Selected Topics in Applied Earth Observations and Remote Sensing*, 11, 2127-2133.

Watanabe, M., Koyama, C. N., Hayashi, M., Nagatani, I., Tadono, T., Shimada, M., 2021. Refined algorithm for forest early warning system with ALOS-2/PALSAR-2 ScanSAR data in tropical forest regions. *Remote Sensing of the Environment*, 265, 112643.